An operando-IR study of photocatalytic reaction of methanol on new *BEA supported TiO2 catalyst

Mohamad El-Roz, Philipe Bazin, Frederic Thibault-Starzyk

An Operando-IR study of photocatalytic reaction of methanol on new *BEA supported TiO_2 catalyst

Mohamad El-Roz*, Philipe Bazin, Frederic Thibault-Starzyk

Laboratoire Catalyse et Spectrochimie, ENSICAEN, Université de Caen, CNRS, 6 Bd Maréchal Juin, F-14050 Caen, France

** Corresponding author*

Abstract

Operando-IR was used to study the photocatalytic oxidation of methanol in gas phase using a new *BEA zeolite supported TiO_2 (*BEA-Ti) photocatalyst. Following the photocatalytic reaction with time resolved IR spectroscopy coupled to mass spectrometry allowed a quantitative and mechanistic study. The surface species and the parameters affecting the reactivity and selectivity of the reaction were identified and a mechanism was proposed. For comparison, *BEA zeolite and TiO_2 (P25) compounds have been examined as photocatalysts. The effect of the temperature on the reactivity and selectivity of the photooxidation was investigated by TPD measurements (from RT to 473K). The new *BEA-Ti material showed high reactivity, despite its low content in TiO_2 (~10%).

Keywords: operando-IR; methanol photooxidation; TiO_2 photocatalyst; Beta zeolite; photocatalyst reactivity; photocatalyst selectivity; reaction mechanism

Introduction

The growing concern in the general public as well as the increased severity of air control regulations give increasing interest to the removal of Volatile Organic Compounds (VOC). One of the key features for such removal is the use of heterogeneous catalysts, largely used for the control and treatment of exhaust gases in the chemical and car industries. The reaction on the catalyst can be induced by heating, or by UV light when using a photocatalyst, with advantages such as low cost, excellent efficiency and low environmental impact.

Titanium dioxide TiO_2 has high photoactivity, it is resistant to photocorrosion, photostable and non toxic. It is largely used for the purification of water or air. [1–5] Supporting TiO_2 on another solid can be very interesting for controlling the dispersion and particle size of TiO_2, for improving its specific surface, which are key factors in catalytic activity. Many different methods have been employed, and TiO_2 has been supported on fiberglass,[6-7] on activated charcoal,[8-10] and on zeolites.[11-15] Zeolites are often considered as the ideal support because of their pore distribution, their high adsorption capacity and their eco-friendliness. Their tuneable hydrophilicity and hydrophobicity allow excluding unwanted ions (heavy metals) and molecules from the reaction site (e.g. residual organic pollutants formed during the photodégradation reaction). On the other hand, TiO_2 supported on zeolite allow the reactivation of the porosity of these precious materials, from adsorbed organic compounds, by photocatalytic way. These complementary characteristics of zeolite and TiO_2 make the coupling of both materials very important for wide applications: purification of water and air, photoactivation of zeolites after catalytic reactions...

Zeolite based TiO_2 photocatalysts are often prepared by Solid State Dispersion (SSD) of TiO_2 on zeolite[14] or by introducing Ti during the sol-gel synthesis of the zeolite.[15] A new method for the preparation of TiO_2 on zeolites has been designed recently in our laboratory, by treating zeolites for a

short time (less than 10 min) under a plasma generated with $TiCl_4$ as a precursor. A new photocatalyst was prepared by supporting TiO_2 on beta zeolite (*BEA-Ti), it presents a very high dispersion (10 times more than the catalyst prepared by SSD) and contains covalent bonding between titanium dioxide and zeolitic defects inside the pore system. The detailed preparation method and the complete characterization are presented in another publication.[16]

During a catalytic reaction, operando spectroscopy allows monitoring events taking place on and inside the catalyst in real time. Infrared spectroscopy (IR) is for that purpose very appropriate since it is fast and sensitive. It has been successfully used for studying photocatalysis with various techniques, as for example attenuated total reflection and diffuse reflection.[18-21] The coupling of IR with on line analysis of the products by Mass Spectrometry (MS), Gas Chromatography (GC) or gas IR allows checking that the experiment is performed under operando conditions by identifying and quantifying species coming out of the reactor and by measuring conversion and selectivity.

The work presented here is an IR operando study of the photooxidation of methanol under UV irradiation on the new photocatalyst, *BEA-Ti. Results have been compared with those obtained on pure TiO_2 and on pure beta zeolite (*BEA). These measurements were done on self supporting wafers of the catalysts, in a setup allowing conditions very close to those of the real reaction and giving quantitative results. The influence of temperature was studied in real time from room temperature to 873 K, with on line analysis of the products by MS.

Experimental

Synthesis and post synthesis treatment

Nanosized Beta crystals (*BEA) were synthesized from a colloidal precursor suspension having the following chemical composition: 0.35 Na_2O : 4.5 $(TEA)_2O$: 1 Al_2O_3: 25 SiO_2 : 295H_2O. The silica source for the preparation of the initial precursor suspension was freshly freeze-dried colloidal silica Ludox SM 30 (30 wt.%), Aluminum isopropoxide (98%, Aldrich) was used as an alumina source and tetraethylammonium hydroxide (TEAOH, 20 wt.% in water, Merck) as a structure-directing agent. These components were mixed under vigorous stirring for 15 min and aged on an orbital shaker at ambient temperature for 24 h prior to the hydrothermal (HT) treatment. The syntheses were performed at 373 K for 11 days. The nanosized crystals resulting from the hydrothermal treatment of the colloidal suspension were purified by three steps centrifugation (20,000 rpm, 60 min), decanting of the supernatant and redispersion in doubly distilled water using an ultrasonic bath. The resulting suspension was then freeze-dried to recover the sample in powder form. The *BEA zeolite crystals were then calcined to remove the organic template. The calcination process consisted of heating the samples from RT to 823 K with a heating rate of 1.75 K/min, keeping at this temperature for 5 hours and then cooling down to room temperature in 5 hours.

The incorporation of TiO_2 in this material has been performed by a new post-synthesis method. The detailed description of this method and the characterization of the obtained catalyst is described and reported separately in reference [16]. According to the TEM and EDS analyses performed on the resulting compound, the amount of TiO_2 has been estimated to ~10% (w/w) with a homogeneous dispersion.

In order to show the efficiency and the performance of the *BEA-Ti photocatalyst prepared by the new method, photooxidation of methanol has been carried out. As a comparison, the photooxidation has been also performed on a reference *BEA sample (the same sample used for the post syntheses

treatment) and a commercial TiO_2 from Degussa (P25, specific surface area = 55 m^2/g).

Conditions for Photocatalytic operando test

The photocatalytic oxidation of methanol has been followed by IR spectroscopy. The powder of the desired catalyst was pressed into self-supported wafers (Ø = 16 mm, m~10 mg cm^{-2}), and experiments were carried after activation of the pellet at 473 K for two hours and then colding down to RT. IR spectra were collected with a Nicolet 5700 FT-IR spectrometer (64 scans/spectrum) equipped with a MCT detector. The operando system is connected to a flow set-up. Gases are introduced into the lines (heated at 333 K) by mass flow controllers. The two gas mixtures, so called "activation" and "reaction" flows, can be prepared and sent independently to the reactor cell. The "Sandwich" reactor-cell used in this study is an evolution of the *operando* cell developed by Saussey et al.[22,23], which has proved its reliability over many years of *operando* studies[22-30], It is made of a stainless steel cylinder that carries a toroidal sample holder in its centre, where the catalyst is placed in the form of a self supported wafer of ~10 mg cm^{-2}. Tightness is obtained by Kalrez© O-rings, and the dead volume (typically defined as the residual space between each sample face and the windows) is reduced to about 0.4 ml by filling the empty space with KBr windows placed at each side of the sample holder. In such a way the surface analysis without superposition of the gas phase signal is made possible and fluid dynamics is very similar to that of a honeycomb system. Gases are introduced on the sample by 1/8" OD pipe and collected on the opposite side of the sample holder. More details can be found in the following references [22,45]. For this specific photocatalytic oxidation study, UV irradiation was carried out with a polychromatic light of a Xe-Hg lamp (LC8 spot light Hamamatsu, L10852, 200 W). It has been performed by using a UV-light guide (A10014-50-0110) mounted at the entrance of the IR operando cell as presented in Scheme 1 in order to establish a homogeneous irradiation. UV irradiation intensity (I_0) has been measured using a light power meter (from Hamamatsu).

In such a configuration, the working pressure was set to atmospheric pressure and, in order to simulate the little amount of VOC to be removed from ambient air, a low partial pressure of methanol was established using a saturator at a carefully controlled temperature. The gas mixture composition was then fixed to 1 vol.% CH_3OH, 20 vol.% O_2 in argon and the total flow was adjusted to 25 cm^3/min. Before any experiment, each sample was treated with argon and oxygen at 473 K for two hours. In order to evaluate the reaction product yields, the IR spectrometer was coupled with a mass spectrometer.

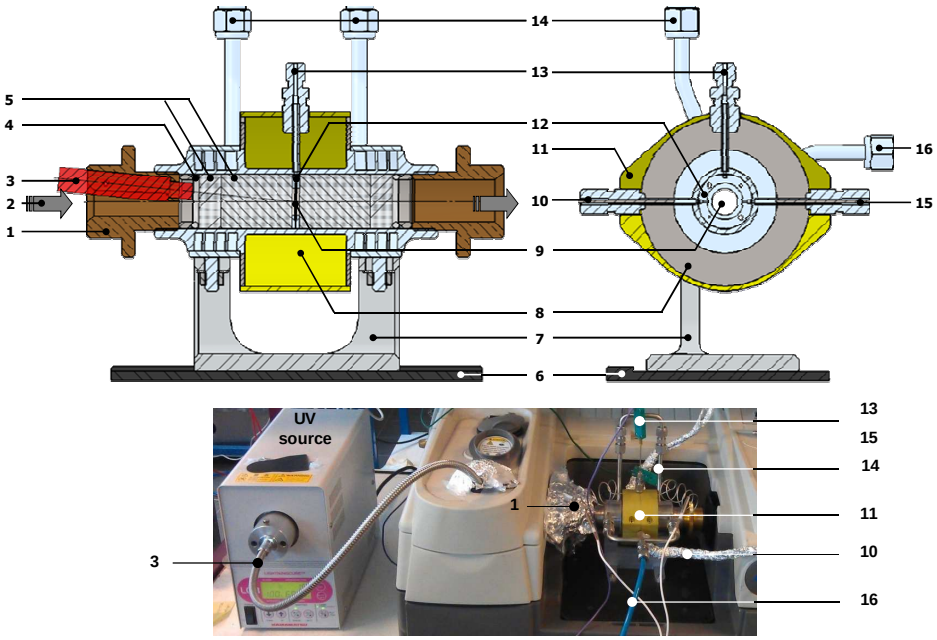

Scheme 1 Longitudinal (Top-left) view, radial (Topright) view and picture (bottom) of the sandwich reactor-IR cell modified for UV catalysis study. 1 - Adjusting nut for airtightness (modified for UV-guide position), 2 - IR *BEAm, 3 -UV-light guide, 4 – Kalrez O-ring, 5 – KBr windows, 6 - Spectrometer base-plate, 7 - IR cell support, 8 – Oven location, 9 – Sample (wafer), 10 - Gas inlet, 11 - External shell, 12 - Wafer holder, 13 - Thermocouple location, 14 - Air cooling outlet, 15 - Gas outlet, 16 – Air cooling inlet.

Results and discussion

IR study of methanol photooxidation

Surface species identification

The photooxidation of methanol has been performed under same reaction conditions (concentration, temperature, flow rate…) using three types of catalyst; *BEA-Ti, *BEA zeolite and TiO_2 (Degussa P25). Figure 1 shows the IR spectra of *BEA and *BEA-Ti samples monitored at RT after saturation with methanol, before and during UV irradiation.

Before UV irradiation, *BEA-Ti spectrum (Figure 1-ii) displays two bands at 2831 cm^{-1} and 1450 cm^{-1} that are absent in the spectrum of *BEA (Figure 1-iv). These two bands correspond respectively to the $\nu(CH_3)$ and $\delta(CH_3)$ vibration modes of dissociativly chemisorbed methanol (with rupture of the O-H bond) on TiO_2 surface (denoted as (b) in Figure 1).[31-33] The shift of these bands (close to 5 cm^{-1}) compared to the literature could be attributed to the influence of the zeolite framework on the vibration of methanol adsorbed on TiO_2. The relatively high intensity of these two bands compared to those observed in TiO_2 spectrum (Figure 2) is due to a high and homogeneous dispersion of TiO_2 in *BEA zeolite structure. The additional bands present in both *BEA and *BEA-Ti spectra in absence of irradiation are attributed to methanol molecularly adsorbed on *BEA zeolite structure (denoted as (a) in Figure 1). The band broadening at 2955-2948 cm^{-1} in *BEA-Ti spectrum is due to the overlap of $\nu(CH_3)$ of physisorbed methanol on the surface of *BEA structure (2952 cm^{-1}) with that adsorbed on the incorporated TiO_2 particles (2948 cm^{-1}).

UV-irradiation induces no change in the IR spectrum of *BEA sample (Figure 1; iii-iv), while several new bands appear in the spectrum of *BEA-Ti (Figure 1; i-ii). The bands at 2973 cm^{-1}, 2896 cm^{-1}, 1508 cm^{-1} and 1750 cm^{-1} can be assigned respectively to $\nu_{as}(CH_2)$, $\nu_s(CH_2)$, $\delta(CH)$ and $\nu(CO)$ vibration modes of adsorbed formaldehyde [25] (denoted as (c) in Figure 1) and those at 1580-1650cm^{-1}, 1490 cm^{-1}, 1405 cm^{-1} and 1365 cm^{-1} to $\nu_{as}(COO)$, $\delta(CH_2)$, $\omega(CH_2)$ and $\nu_s(COO)$ vibrations of mono- and bi-dentate formate species [22, 25-27] (denoted as (d)). The additional bands at 1717 cm^{-1} and 1380 cm^{-1} can be attributed respectively to $\nu(CO)$ and $\nu(CH)$ vibrations of adsorbed formic acid [34] (or methyl formate) (e). The bands at 2948 cm^{-1} and 1672 cm^{-1}, are probably due to more strongly adsorbed formic acid or methyl formate species (f). These bands can be assigned respectively to $\nu(CH)$ and $\nu(CO)$ of $HCOOH$ or $HCOOCH_3$ coordinately bonded to the Lewis acid sites.[34,37] It is important to note that the carbonyl stretching frequencies observed for *BEA-Ti sample are lower (~10 cm^{-1}) than those reported in the literature for formic acid or methyl formate adsorbed on TiO_2 surface [34-36] due to the zeolitic influence.

The IR spectra of TiO_2 sample before and during UV irradiation are reported in Figure 2. New bands appear at 1555 cm^{-1}, 1504 cm^{-1}, 1405 cm^{-1} and 1358 cm^{-1}. These bands are assigned respectively to $\nu_{as}(COO)$, $\delta(CH_2)$, $\omega(CH_2)$ and $\nu_s(COO)$ vibrations of bidentate formate species adsorbed on the catalyst surface.[34-37] Their relatively low intensity during UV irradiation (compared to those of *BEA-Ti) could be explained by the relatively low acidity and specific area of TiO_2 leading to a relatively low adsorption and/or low selectivity of the photocatalytic reaction.

Time evolution of surface species

The evolution of the IR spectrum of *BEA-Ti sample during the first 35 min of UV irradiation is reported in Figure 3A. It shows an increase in the intensity of the bands assigned to formic acid (1717cm^{-1}) (or methyl formate) and bidentate formate species (1585 cm^{-1}) adsorbed on the surface. Figure 3B represents the evolution of the integrated surface areas of these two bands versus irradiation time. The band area of $\nu(CO)$ vibration (1760-1690 cm^{-1}) reached a plateau after only 5 minutes while that of formate species (OCO) (1690-1500 cm^{-1}) took 35 min to reach the plateau. By evaluating the constant rates of these two emerging species, it has been observed that the production of CO species (formic acid or methyl formate) is twice faster than that of OCO species (formate species). This can be explained by the transformation of formate species to either formic acid or to methyl formate which leads to an apparently lower rate constant than that of the formation of $HCOOH$ (or $HCOOCH_3$). Moreover, the plateau of the band of $\nu(CO)$ vibration observed after 5 min of irradiation is explained by the reach of the adsorption/desorption equilibrium of $HCOOH$ (or $HCOOCH_3$).

Table 1 summarizes the vibration modes of the different species observed in this study.

On line MS analysis of products and UV irradiation intensity effect

The influence of UV irradiation intensity (I_0) on the photooxidation of methanol has been investigated for the three samples. The conversion of methanol has been followed by the evolution of the MS signal m/z=31. Figure 4 shows the evolution of the methanol conversion vs I_0 for the three samples. When *BEA is used as photocatalyst, no photooxidation occurs even with the increase of irradiation intensity (Figure 4A). Such a result is in good agreement with the IR results discussed above.

The methanol conversion in the case of *BEA-Ti and TiO_2 increases with increasing I_0. For I_0< 5.1 mW/cm^2, the conversion of methanol with *BEA-Ti and TiO_2 are close. The difference becomes more important when I_0 is higher than 5.1 mW/cm^2. In this case the maximum methanol conversion on *BEA-Ti catalyst is 20% while that obtained on TiO_2 is 40%. This could be attributed to the difference in UV-absorption in the region of the lamp emission (most important at 365 nm and 314 nm) of these two materials (Figure 5).

Such a hypothesis is well confirmed by the change in the aspect of the curve, representing the evolution of methanol conversion vs I_0, on *BEA-Ti sample when I_0 > 5.1 mW/cm^2 (which is not the case for TiO_2) (Figure 4A).

Even though the direct comparison of the photocatalytic activity of these two samples is not evident (due to the different properties of these two samples), *BEA-Ti shows a relatively high efficiency (~50% compared to TiO_2) with only ~10 wt.% of incorporated TiO_2.

Moreover, the absence of photocatalytic activity for *BEA sample confirms that the zeolite structure has no direct impact on photooxidation. It could have a negative effect on the UV absorption. But it probably plays a positive role by increasing the specific surface area of the catalyst dispersed into the structure. In addition, the well known acidic properties of *BEA zeolite [39-42] could also improve the photocatalyst/organic compound interaction and improve the adsorption of this latter hence the photoreactivity.

The evolution of the MS intensity of m/z= 18, m/z=44 and m/z= 45 vs I_0 for *BEA-Ti and TiO_2 (P25) is reported in Fig. 4B. As shown in this Figure, zeolite can also affect the selectivity of the reaction. The photooxidation of methanol in the presence of TiO_2 resulted in two main signals at m/z=18 and m/z= 44. These two signals have been attributed respectively to H_2O and CO_2. This result reveals that the main reaction on TiO_2 is photo-combustion.

On the other hand when *BEA-Ti is used, the CO_2 signal was found to be 3.2 to 4.4 times less important than that on TiO_2. According to the results discussed above (the conversion rate of methanol with TiO_2 found to be two times more important than that with *BEA-Ti, Figure 4A), the ratio TiO_2 /*BEA-Ti of this signal must be close to 2. This difference (3.2-4.4 in place of 2) is explained by the presence of other types of reaction with *BEA-Ti where a signal MS at m/z=45 occurred (it is ~26 times less important with TiO_2) (Figure 4A). This latter can be assigned to the production of either formic acid or methyl formate. In our MS conditions, the ratio of the MS signal (m/z=45)/(m/z=46) was found to be equal to ~30. The theoretical ratio (m/z=45)/(m/z=46) for formic acid is close to 0.8 and that of methyl formate is more than 30. As a conclusion, the species generated during the photooxidation on *BEA-Ti is without any doubt the methyl formate and not the formic acid. This reaction stands for a ~50% of the total conversion of methanol with *BEA-Ti (estimation based on the ratio of CO_2 produced in the case of TiO_2 and *BEA-Ti after taking into account the conversion rate of methanol). These results are in a good agreement with the IR results reported in Figures 1, 2 and 3 that showed a relatively high selectivity to methyl formate with *BEA-Ti and to photocombustion with TiO_2 under our conditions.

In this part, MS analysis was used to determine the conversion of the reaction, to determine its selectivity and to detect the photocombustion of methanol. In the case of *BEA-Ti, the reaction passed by two pathways; the formation of methyl formates (~50%) and photocombustion (~50%). In the case of TiO_2, the major reaction was the photocombustion. By considering the mass weight of TiO_2, TiO_2 particles present in *BEA-Ti (~10 wt.%) were found to be 5 times more reactive than TiO_2 P25.

Mechanism

Based on the results reported above, a mechanism for the photooxidation of methanol could be suggested as follows:

$TiO_2 + h\nu \rightarrow h^+ + e^-$ ($h^+ + e^-$ = electron-hole pair) (1)

in the presence of O_2

$O_2 + e^- \rightarrow O_2^{\bullet -}$ (2)

Methanol and methoxy species adsorbed ($CH_3O_{(a)}$) on the catalyst surface can react directly with the holes (h^+) as already reported in the literature [43,44]:

$CH_3O^- + h^+ \rightarrow CH_3O^{\bullet}_{(a)}$ (3)

$CH_3O^{\bullet}_{(a)} \rightarrow CH_2O^{\bullet -}_{(a)} + H^+$ (4)

$CH_2O^{\bullet -}_{(a)} \rightarrow H_2CO_{(a)} + e^-$ (5)

In the presence of $O_2^{\bullet -}$ the formaldehyde could be oxidized into CO_2 and H_2O (photocombustion):

$H_2CO + O_2^{\bullet -} \rightarrow CO_2 + H_2O + e^-$ (6)

$CH_3O_{(a)}$ and $CH_3OH_{(a)}$ can be oxidized to form bidentate formate species $HCOO_{(a)}$:

$CH_3O_{(a)} + O_2^{\bullet -} \rightarrow HCOO_{(a)} + H_2O + e^-$ (7)

HCOO in presence of CH_3O leads to the formation of methyl formate:

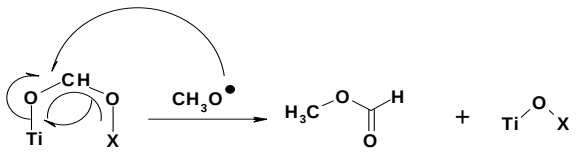

X= Ti, Si or Al (8)

Effect of temperature on the photooxidation

The photooxidation of methanol has been performed at a variable temperature between RT to 473 K with a heating rate of 2 K/min. The reaction has been performed under the same experimental conditions mentioned above and followed by IR and on line MS analysis. The UV intensity is fixed close to 10 mW/cm^2.

As predicted, no photocatalytic effect was observed for the *BEA sample at a temperature ≤ 473 K.

The evolution of the subtracted IR spectrum (from the spectrum at RT) and the IR bands height for adsorbed species on *BEA-Ti vs temperature without (UV-OFF) and during (UV-ON) UV irradiation are shown at Figure 6.

In the absence of UV irradiation (UV-OFF), the intensity of the band at 2830 cm^{-1}, assigned to chemisorbed methanol (Table 1), increases with temperature. It stabilizes when the temperature reaches 343 K (Figure 6-A). The methanol chemisorption on TiO_2 surface was favored with the heating. The decrease of the remaining (CH) bands is due to desorption of physi- and chemisorbed methanol on the acidic sites of *BEA-Ti. When the sample is irradiated (Figure 1), (UV-ON), the bands corresponding to methyl formate, formaldehyde and formate species appear (Figure 6-B). The evolution of the height of these bands vs temperature shows that the temperature favors the desorption of all of the species adsorbed on the surface of *BEA-Ti (even the chemisorbed methanol). The desorption of these species is accompanied by a decrease of the large band between 3600-3000 cm^{-1}, attributed to terminal ν(OH) bonded to adsorbed species via hydrogen bonding. The release of these sites is translated by the manifestation of a narrow vibration band at 3740 cm^{-1} that corresponds to terminal isolated silanol (ν(SiOH)) vibration (Figure 6-I).

The same phenomenon has also been observed in the case of TiO_2. Without UV irradiation (UV-OFF), the bands at 1315, 2821 and 2924 cm^{-1} assigned to chemisorbed methoxy groups (Table 1) increase with temperature (Figure 7). Physisorbed methanol (1567, 2834, 2950 cm^{-1}) follows the same evolution as the chemisorbed methoxy groups (2921 cm^{-1}, 2951 cm^{-1}) but in the opposite direction (decreases). Thus, the chemisorption of methanol on TiO_2 first implies physisorption.
During UV irradiation (UV-ON; Fig. 7-B), the evolution of the IR bands height at 1750 cm^{-1}, 1663 cm^{-1} and 1367 cm^{-1} (attributed to formaldehyde and bidentate formate species) and those at 2846 cm^{-1} (attributed to physisorbed methanol) vs temperature are symmetrical. This shows that the decrease of the bands for physisorbed methanol stands not only for desorption of methanol but also for the photooxidation of methanol. On the other hand, the evolution of bidentate formate bands at 1550 cm^{-1} and 1330 cm^{-1} and that of chemisorbed methanol at 2921 cm^{-1} and 2951 cm^{-1} show also a similar behaviour, and temperature favours the generation of bidentate formate species from chemisorbed methanol. The generated species (chemisorbed formate species) can then undergo either a total oxidation to CO_2 and H_2O or remain adsorbed on the surface (Figure 7). In this case the efficiency of the TiO_2 is affected; it decreases with the increase of chemisorbed species on the surface.
The evolution of the MS signal of the different generated species vs temperature for *BEA-Ti and TiO_2 is shown in Figure 8: Photooxidation activity increases, in general, with the temperature.
First, the conversion of methanol into CO_2 (m/z=44) and H_2O (m/z=18) (photocombustion) (Figure 8-A) with TiO_2 reaches a maximum at about ~423K. This can be explained by the decrease of activation energy of the photocombustion of methanol. A slight decrease of the photocatalytic activity appears also between 443 K ≤T≤ 473 K. This observation is in a good agreement with the IR results that showed an increase of the chemisorbed species for T> 433 K (Figure 7-B-II). In the case of *BEA-Ti, the formation of methyl formates (m/z=45) reaches the maximum at 383±5 K. In addition, at a temperature > 393 K, the photocombustion of methanol becomes dominant. At high temperature, it favors either the formation of methyl formate or the photocombustion. At T> 460 K, the formation of methyl formate returns to its initial level observed at room temperature. This means that the increase of the conversion of methanol in this case results from the increase of photocombustion.

Figure 9 shows the evolution of methanol conversion with temperature using TiO_2 (a) and *BEA-Ti (b). The evolution of $(CO_2)_{*BEA\text{-}Ti}/(CO_2)_{TiO2}$ ratio normalized for the same methanol conversion is also reported in this figure. This ratio with a value different from 1, explains the presence of other secondary reactions (the methyl formate formation discussed above). The change of this ratio with the temperature proves that the temperature affects the selectivity of the photooxidation of

methanol on *BEA-Ti. Moreover for a temperature between 410 K and 450 K, a stabilization of the conversion of methanol is observed (Figure 9). This is due to the decrease of methyl formate formation that is accompanied by the increase of the formation of CO_2 and H_2O. This agrees with the IR results that showed a minimum of adsorbed methyl formate on *BEA-Ti for T > 390 K (Figure 10).
For T > 438 K the conversion rate of methanol decreases on TiO_2 while it continues to increase on *BEA-Ti. This observation agrees with the IR results discussed above (Figure 6-B) showing that the temperature favours the desorption of the different chemi- and physisorbed species on the surface of *BEA-Ti. Furthermore, when the temperature reaches 473 K for *BEA-Ti, the MS signal m/z=45 returns to its initial level at RT. Since the increase of photocombustion not lead to a decrease in the production of methyl formate. These results, suggest that the formation of methyl formate species takes place on characteristic sites of *BEA-Ti (e.g. on TiO_2 present in the micropores or on TiO_2 bonded to acidic sites…).
At a temperature ≤ 473 K and in absence of UV irradiation, no reaction has been observed for all of the three samples investigated in this work. It should be noted that the work has been done at T ≤ 473 K to avoid the transformation of TiO_2 at high temperature.
These results confirm the influence of the temperature on the reactivity of the photooxidation of methanol in the case of *BEA-Ti and TiO_2 and on the reaction selectivity in the case of *BEA-Ti.

Conclusions

A new operando setup has been made to study the photooxidation of methanol (1% in synthetic air) on a new elaborated photocatalyst. Two types of photocatalyst have been investigated TiO_2 (P25-Degussa) and *BEA supported TiO_2 (*BEA-Ti). It highlights the interesting reactivity of *BEA-Ti compound. With only ~10 wt.% of incorporated TiO_2, *BEA-Ti showed a relatively high efficiency (50%) compared to TiO_2. By considering the mass weight of TiO_2, the reactivity of TiO_2 presented in *BEA-Ti was 5 times higher than that of TiO_2–P25. For comparison, *BEA zeolite has been also investigated as photocatalyst. It did not show any photooxidation activity. The selectivity of TiO_2 and *BEA-Ti photocatalysts was found to be different. While the major reaction observed in the case of TiO_2 was the photocombustion, the formation of methyl formate species in case of *BEA-Ti contributed to ~50% of the photooxidation (vs ~50% of photocombustion reaction). The increase of the UV-irradiation intensity increases the reactivity. The methanol photooxidation mechanism over TiO_2 and *BEA-Ti at room and high temperatures has been clarified. Indeed, for TiO_2 photocatalysts, high temperatures (> 443 K) favor the chemisorption and led to a weak decrease in the reactivity. On the contrary, for *BEA-Ti, the increase of the temperature increases the conversion of methanol and the reactivity. This result has been assigned to the poisoning of TiO_2 surface at high temperatures under our condition which not the case of *BEA-Ti.

Figures and Tables.

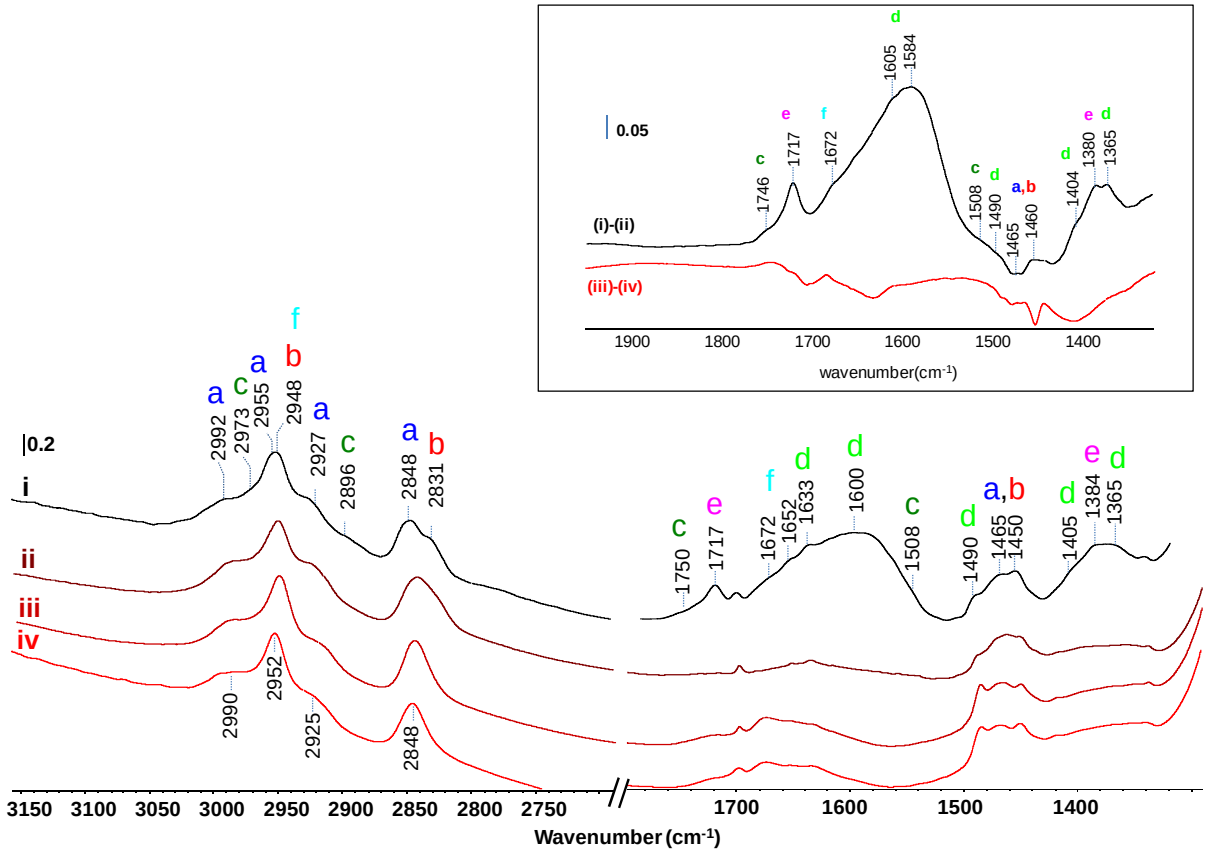

Figure 1: **IR spectra recorded after methanol adsorption on *BEA-Ti (i-ii) and *BEA (iii-iv) zeolite before (ii, iv) and during (i, iii) UV irradiation. Spectra were acquired at RT. Insert: Subtraction results of *BEA-Ti (i-ii) and *BEA (iii-iv).**

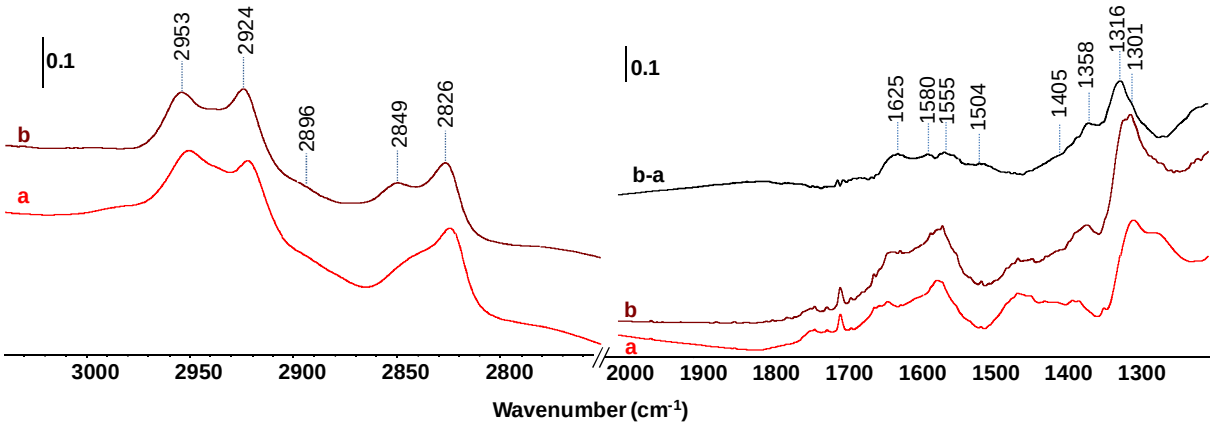

Figure 2: **IR spectra recorded after methanol adsorption on TiO_2 (P25) before (a) and during (b) UV irradiation. Spectra were recorded at RT. (b-a): Subtraction results.**

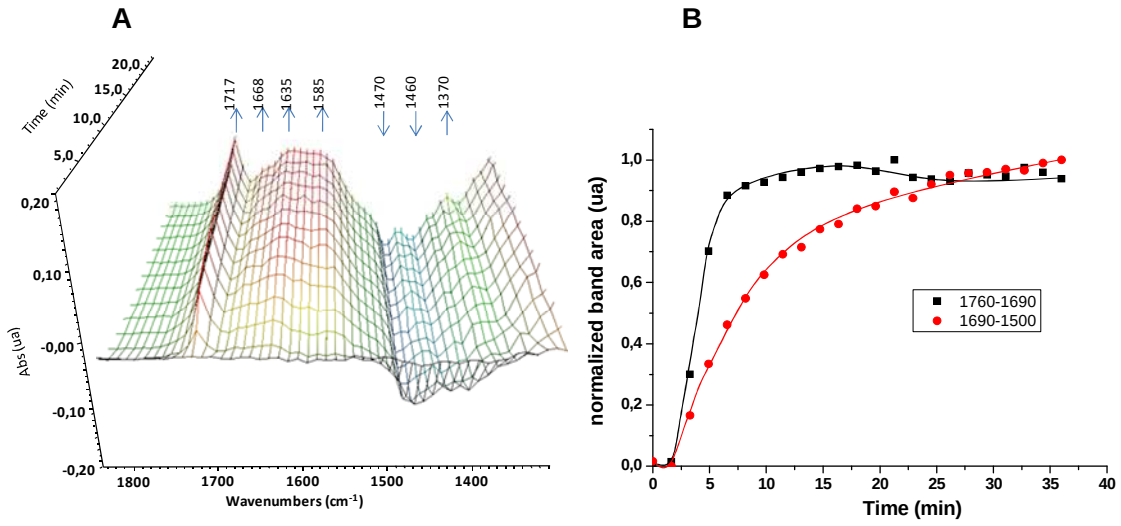

Figure 3: (A) Evolution of IR spectra at RT during methanol photooxidation (1% of methanol in N_2/O_2 20%/79% vol.%, 25 cm^3/min) vs time of the species adsorbed on *BEA-Ti during UV irradiation (subtraction result from the spectra before irradiation). (B) Evolution of integrated band area of (CO) and formate species (OCO) during UV irradiation. t=0 corresponds to the time when irradiation has been established.

	(cm^{-1})					
	a Physisorbed methanol 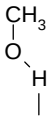	b Chemisorbed methanol 	c Physisorbed formaldehyde 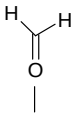	d formate species 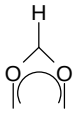	e Physisorbed methyl formate 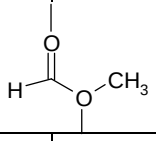	f Methyl formate coordinatiely bonded to Lewis sites
ν_s(CH)	2848 (2849*)	2830 (2825*)	2896	_	_	2896
ν_{as}(CH)	2992; 2927 (2923*)	2955; 2948 (2953*)	2973	_	_	2946
δ_{as}(CH)	1475-1450	1475-1450	1508	1490	1382	1672
ν(CO)	_	_	1750	_	1717	_
ν_s(COO)	_	_	_	1365	_	_
ν_{as}(COO)	_	_	_	1580-1650	_	_
$\omega(CH_2)$	_	_	_	1405	_	_

Table 1 Vibration modes assignment of the major adsorbed species on *BEA-Ti and TiO_2 (*) formed during photocatalytic degradation of methanol.

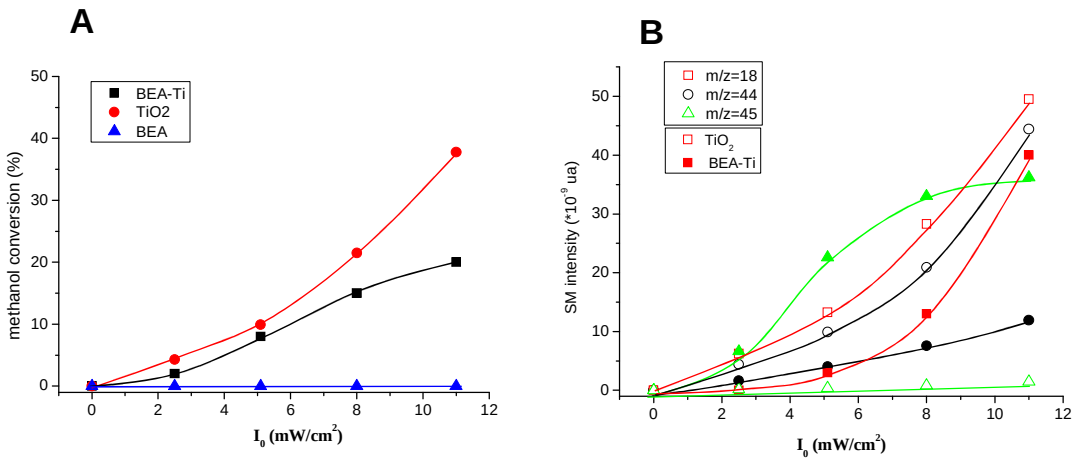

Figure 4: **(A) Evolution of the methanol conversion (in %) vs the UV intensity of the lamp (I_0) using *BEA-Ti (square), TiO_2 (P25) (cercle) and *BEA (triangle) as photocatalyst. (B) Evolution of the MS intensity of m/z= 18 (square), m/z=44 (cercle) and m/z= 45 (triangle) vs I_0 of *BEA-Ti (close symbol and solid line) and TiO_2 (P25) (open symbol and doted line). N.B. the m/z=18 signal has been divised by 5.**

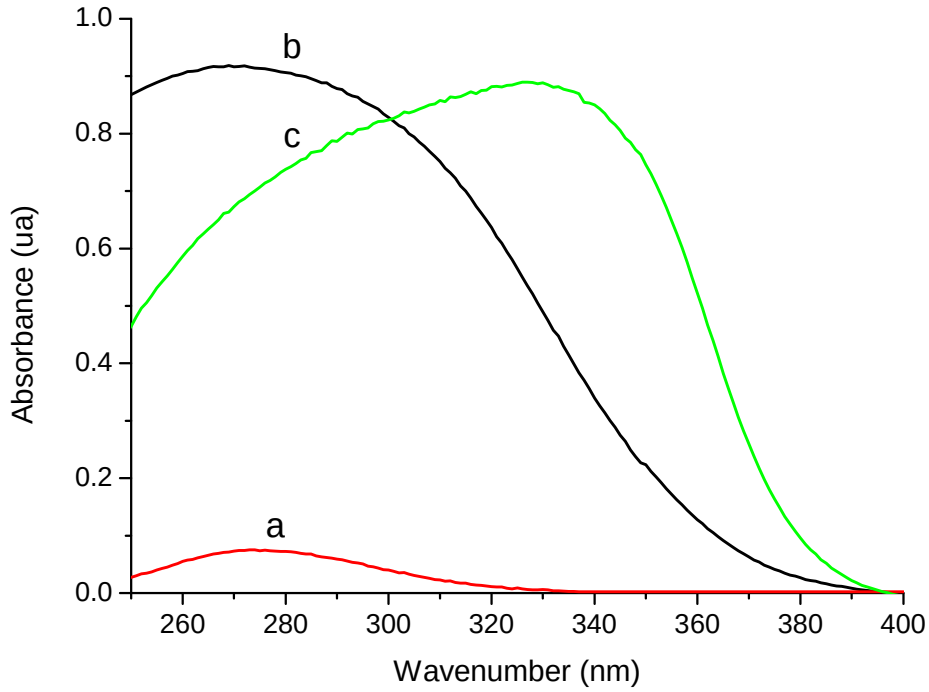

Figure 5: **DR UV-visble spectra of *BEA (a), *BEA-Ti (b) and TiO_2 (P25) (c).**

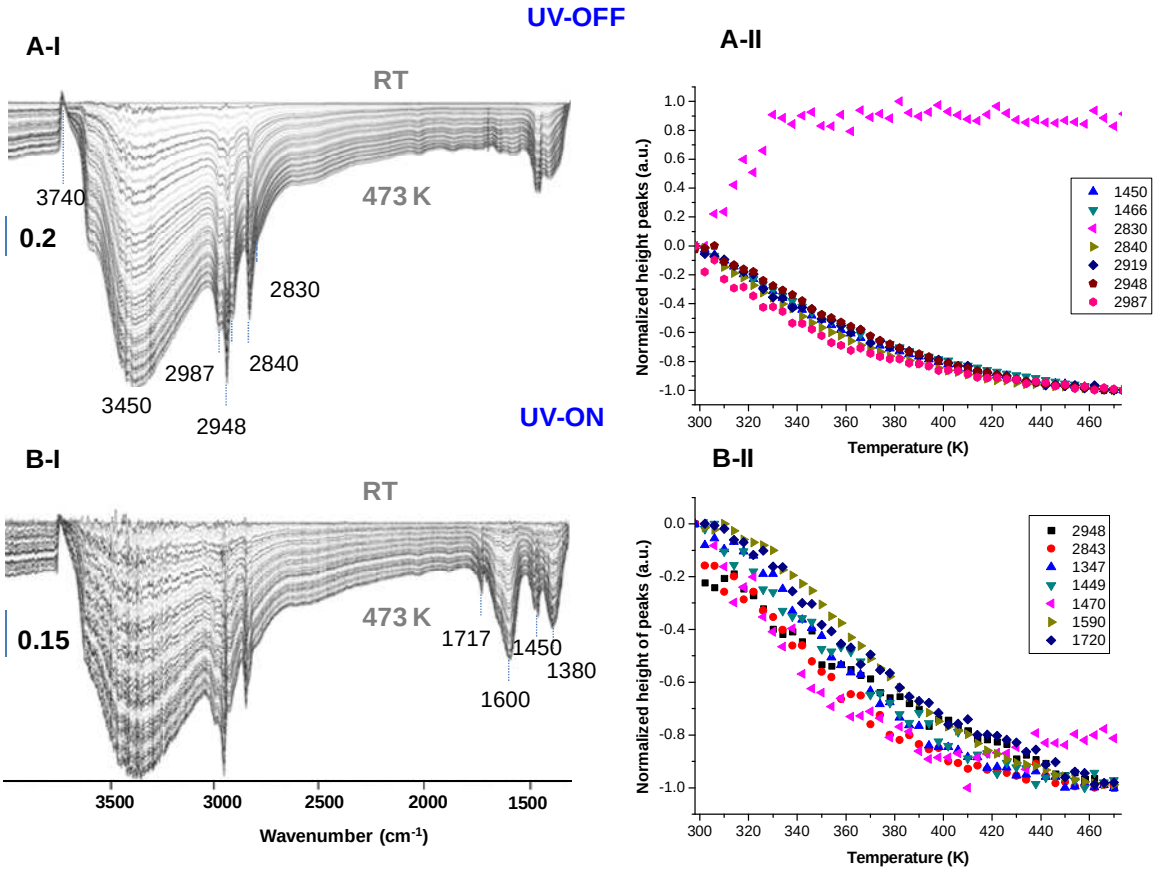

Figure 6: Evolution of sustracted IR spectra (from the spectrum at RT) of methanol adsorbed on *BEA-Ti photocatalyst vs temperature without (A) and during (B) UV irradiation. I) original spectra; II) evolution of the height peaks vs temperature.

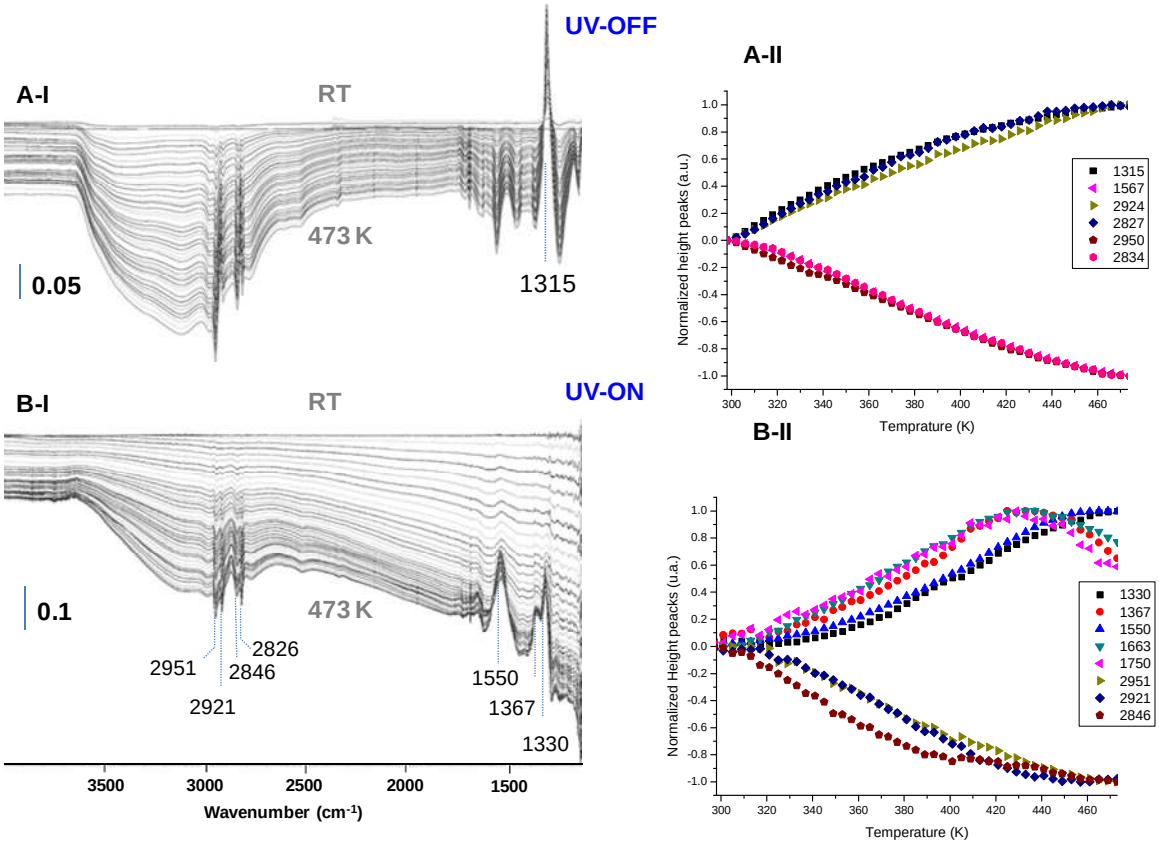

Figure 7: Evolution of subtracted IR spectra (from the spectrum at RT) of methanol adsorbed on TiO_2 photocatalyst vs temperature without (A) and during (B) UV irradiation. I) original spectra; II) evolution of the height bands vs temperature.

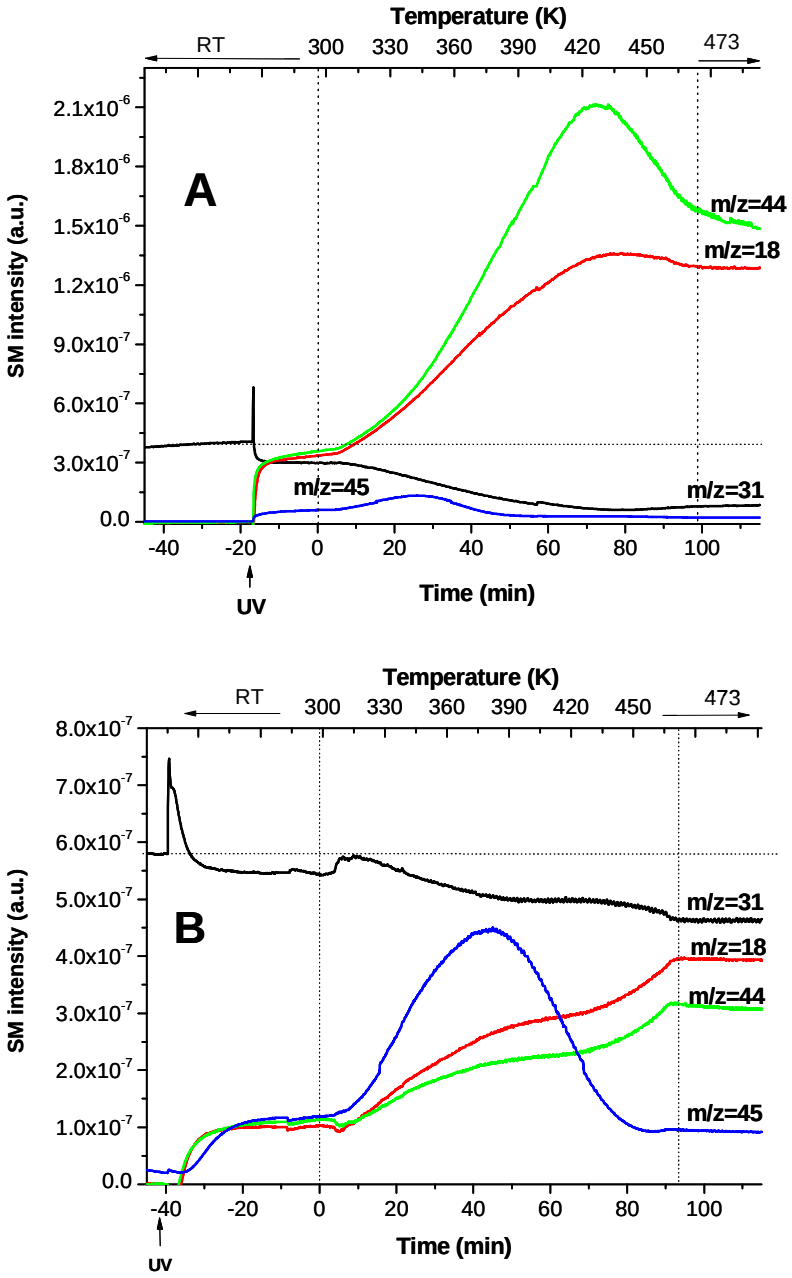

Figure 8: Evolution of MS signal vs temperature during the photoxidation of methanol using TiO_2 (P25) (A) and *BEA-Ti (B) as phoocatalyst. N.B. the signal of m/z=44, 45 has been multiplied by 10.

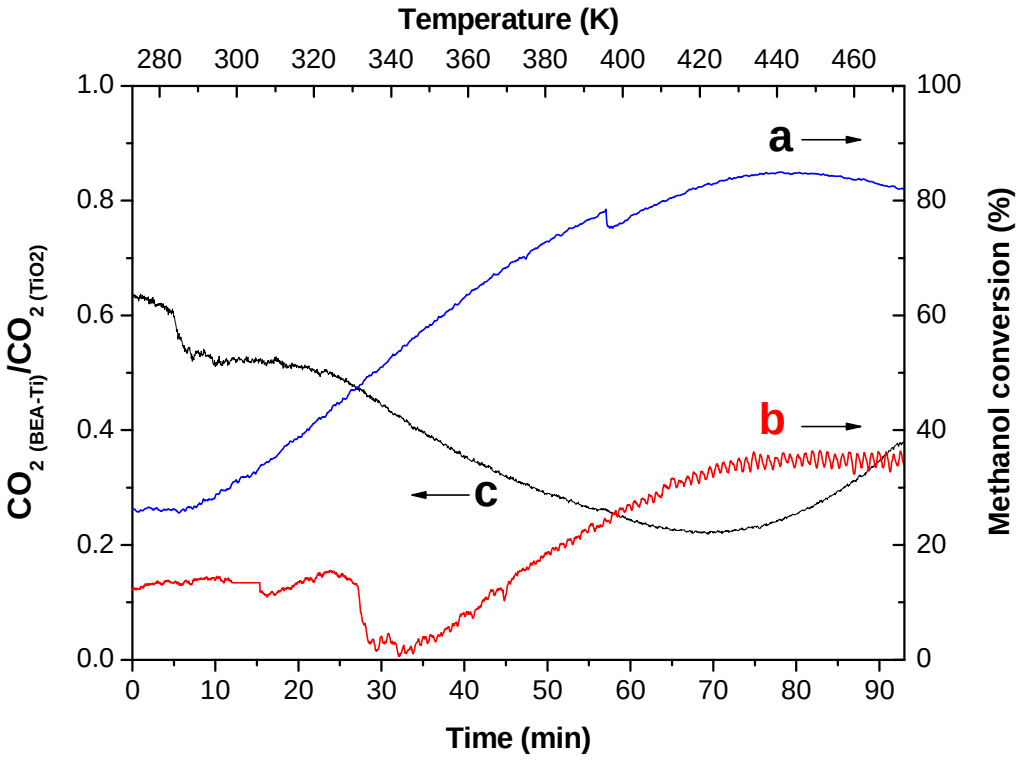

Figure 9: **Evolution of methanol conversion with temperature using TiO_2 (a) and *BEA-Ti (b) as photocatalyst. (c) Corresponds to the $(CO_2)_{*BEA-Ti}$ /$(CO_2)_{TiO2}$ ratio normalized for the same methanol conversion.**

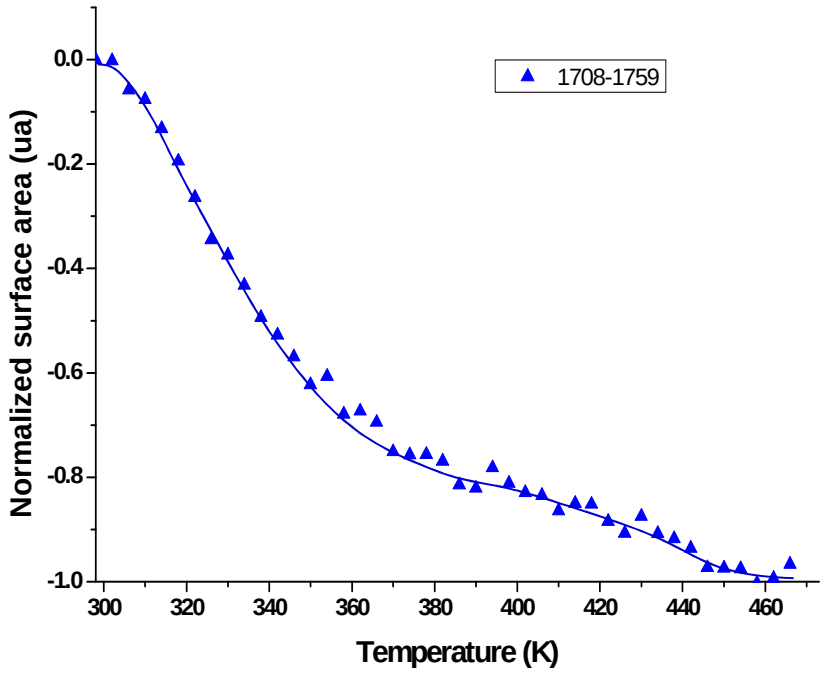

Figure 9: **Normalized surface area evolution of ν(CO) band of methyl formate vs temperature.**

References

1 D.F. Ollis, E. Pelizzetti and N. Serpone, Environ. Sci. Technol. 25 **(**1991) 1522.
2 R.W. Matthews, J. Phys. Chem. 1987, **91**, 3328.
3 A. Fujishima, K. Hashimotoand T. Watanabe, *TiO_2* Photocatalysis. Fundamentals and Applications; BKC, Inc.: Tokyo (1999).
4 D.F. Ollis, H. Al-Ekabi, Photocatalytic Purification and Treatment of Water and Air; Eds., Elsevier: Amsterdam (1993).
5 J.M.C. Robertson, P.K.J. Robertson and L.A. Lawton, J. Photochem. Photobiol. A: Chem. 175 (2005) 51-56.
6 D. Robert, A. Piscoro, O. Heintz and J.V. Weber, Catal. Today 54 (1999**)** 291-296.
7 J. Medina-Valtierra, M. Sánchez-Cárdenas, C. Frausto-Reyes and S. Calixto, J. Mex. Chem. Soc. 50 (2006) 8-13.
8 J.M. Herrmann, J. Matos, J. Disdier, C. Guillard, J. Laine, S. Malato and J. Blanco, Catal. Today 54 (1999) 255-265.
9 H. Hou, H. Miyafuji and S. Saka, Journal of Materials Science 41 (2006) 8295-8300.
10 T. Torimoto, Y. Okawa, N. Takeda and H. Yoneyama , Journal of Photochem. and Photobiol. A: Chem., 103 (1997) 153-157.
11 J. Matos, J. Laine and J.M. Herrmann J. Appl. Catal. B, 18 (1998) 281-291.
12 Y. Kim and M. Yoon J. Mol. Catal. A 168 (2001) 257-263.
13 S. Anandan and M. Yoon J. Photochem. Photobiol. C 4 (2003) 5-18.
14 V. Durgakumari, M. Subrahmanyam, V. Subbaraok, A. Ratnamala, M. Noorjahan and K. Tanaka, Applied catalysis. A : General 234 (2002) 155.
15 M. Lafjah, F. Djafri, A. Bengueddach, N. Keller and V. Keller, Journal of Hazardous Materials 186 (2011) 1218-1225.
16 M. El-Roz, V. Valtchef, J. Al Fallah, J.M. Goupil, F. Thibault-Starzyk, in preparation.
17 S. Rousseau, O. Marie, P. Bazin, M. Daturi, S. Verdier and V. Harle, J. Am. Chem. Soc. 132 (2010) 10832-10841.
18 P.A. Deveau, F. Arsac, P.X. Thivel, C. Ferronato, F. Delpech, J.M. Chovelon, P. Kaluzny and C. Monnet, Journal of Hazardous Materials 144 (2007) 692-697.
19 P.Z. Araujo, C.B. Mendive, L.A. Garcia Rodenas, P.J. Morando, A.E. Regazzoni and M.A. Blesa, D. Bahnemann, Colloids Surf. A 265 (2005) 73-80.
20 J.M. Coronado, S. Kataoka, I. Tejedor-Tejedor and M.A. Anderson, J. Catal. 219 (2003) 219-230.
21 J.T. Carneiro, A.R. Almeida, J.A. Moulijn and G. Mul Phys. Chem. Chem. Phys. 12 (2010) 2744-2750.
22 T. Lesage, C. Verrier, P. Bazin, J. Saussey and M. Daturi, Phys. Chem. Chem. Phys. 5 (2003) 4435-4440.
23 S. Wuttke, P. Bazin, A. Vimont, C. Serre, Y.K. Seo, Y.K. Hwang, J.S. Chang, G. Férey and M. Daturi, personnal communication.
24 T. Lesage, C. Verrier, P. Bazin, J. Saussey, S. Malo, C. Hedouin, G. Blanchard and M. Daturi, Topics Catal. 30/31 (2004) 31-36.
25 F. Romero Sarria, O. Marie, P. Bazin, J. Saussey, J. Lesage, A. Guesdon and M. Daturi, Catal. Today 113 (2006) 87-93.
26 T. Montanari, O. Marie, M. Daturi and G. Busca, Appl. Catal. B: Environ. 71 (2007) 216-222.
27 B.I. Mosqueda-Jiménez, A. Lahougue, P. Bazin, V. Harlé, G. Blanchard, A. Sassi and M. Daturi, Catal. Today 119 (2007) 73-77.
28 T. Lesage, J. Saussey, S. Malo, M. Hervieu, C. Hedouin, G. Blanchard and M. Daturi, Appl. Catal. B: Environ. 72 (2007) 166-177.
29 P. Bazin, O. Marie and M. Daturi, General features of in situ and operando spectroscopic investigation in the particular case of DeNOx reactions, In "Past and Present in DeNOx Catalysis : From Molecular Modelling to Chemical Engineering", P. Granger, V.I. Parvulescu Eds., SSSC 171, Elsevier Ch. 4 (2007) pp. 97-143.
30 M. Ahrens, O. Marie, P. Bazin and M. Daturi, J. Catal. 271 (2010) 1-11.
31 C.C. Chuang, C.C. Chen and J.L. Lin, J. Phys. Chem. B 103 (1999) 2439-2444.
32 J.C. Lavalley and N. Sheppard, Spectrochim. Acta 28 (1972) 2091-2101.
33 G. Busca, A. Elmi and P. Forzatti, J. Phys. Chem. 91 (1987) 5263-5269.
34 G. Ya. Popova, T.V. Andrushkevich, Yu.A. Chesalov, and E.S. Stoyanov, Kinet. Catal. 41 (2000) 805-811.
35 J. Arana, J.M. Dona-Rodriguez, C. Garrigai Cabo, O. Gonzalez-Diaz, J.A. Herrera-Melian and J. Perez-Pena, Appl. Catal. B: Environ. 53 (2004) 221-232.
36 J. Arana, J.M. Dona-Rodriguez, C. Garrigai-Cabo, O. Gonzalez-Diaz, J.A. Herrera-Melian and J. Perez-Pena, Appl.Surf.Sci. 239 (2004) 60-71.
37 C.C. Chuang, W.C. Wu, M.C. Huang, I.C. Huang and J.L. Lin, J. Catal. 185 (1999) 423-434.
38 F. Thibault-Starzyk, A. Vimont and J.P. Gilson, Catal. Today 70 (2001) 227-241.
39 A.Vimont, F. Thibault-Starzyk and J.C. Lavalley, J. phys. chem. B 104 (2000) 286-291.
40 F.R.J. Cannings, Phys. Chem. 72 (1968) 4691-4693.
41 M. Lefrançois and G.J. Malbois, J. Catal. 20 (1971) 350-358.
42 R. Buzzoni, S. Bordiga, G. Ricchiardi, C. Lamberti, A. Zecchina and G. Bellussi, Langmuir 12 (1996) 930-940.
43 A. Yamakata, T. Ishibashi and H. Onishi, Int. J. Photoenergy 5 (2003) 7-9.
44 A. Yamakata, T. Ishibashi and H. Onishi, Phys. Chem.B 107 (2003) 9820-9823.
45 I. Malpartida, E. Ivanova, M. Mihaylov, K. Hadjiivanov, V. Blasin-Aubé, O. Marie, M. Daturi, Catal. Today 2010, 149, 295.